CHEMISTRY OF MATERIALS

Made available for a limited time for personal research and study only License.

pubs.acs.org/cm

Article

Inverse Gas Chromatography Demonstrates the Crystallinity-Dependent Physicochemical Properties of Two-Dimensional Covalent Organic Framework Stationary Phases

Kareem Yusuf,*[,§] Anusree Natraj,[§] Kelvin Li, Mohamed Ateia, Zeid A. ALOthman, and William R. Dichtel*

Cite This: https://doi.org/10.1021/acs.chemmater.2c03448

Read Online

ACCESS | Metrics & More | Article Recommendations | Supporting Information

ABSTRACT: Two-dimensional polymers (2DPs), in the form of layered 2D covalent organic frameworks (COFs), are promising candidates for adsorbent-based separations because their pore sizes, shapes, functionalities, and interlayer stacking arrangements can be tuned by modifying their building blocks. Recently, high-quality single crystals of two 2D COFs exhibited distinct and improved separation characteristics in the gas chromatography (GC) separation of benzene and cyclohexane relative to polycrystalline samples of the same materials. These surprising findings motivate the present study, in which inverse pulse gas chromatography (IGC) was used to characterize the dispersive and specific adsorption properties of the surfaces of single-crystalline and polycrystalline **TAPPy-PDA** COFs for the separation of linear *n*-alkanes as well as a series of standard polar probes. Major differences in separation behavior were again observed that provide insight into how analytes interact with the single-crystalline and polycrystalline 2D COFs. A polarity study based on McReynolds constants revealed the nonpolar nature of the single-crystalline **TAPPy-PDA** COF, whereas the polycrystalline **TAPPy-PDA** COF surface was found to have a slightly polar character. Three common approaches to calculating the specific interaction parameter, I^{sp}, were tested to examine their validity in the context of 2D COFs, revealing that the single-crystalline **TAPPy-PDA** COF possessed an electron donor character that we attribute to the imine nitrogen atoms inside the well-defined pore channels. In contrast, the polycrystalline **TAPPy-PDA** COF showed a relative electron acceptor character, which may be more heavily influenced by interactions between the analytes and dangling bonds or functionalities at grain boundaries. These findings provide a quantitative comparison of 2D COF materials quality by determining the acid−base interactions (represented by the electron donor−acceptor properties), polarity, and other physiochemical parameters. Furthermore, these results indicate the importance of establishing high materials quality for 2D COF samples prior to establishing rigorous structure−property relationships for separation performance.

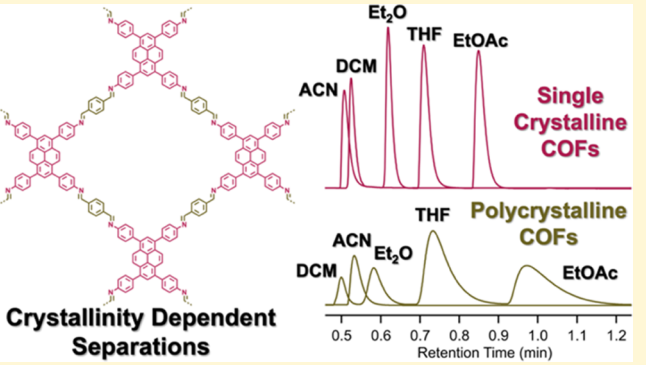

Downloaded via NORTHWESTERN UNIV on February 19, 2023 at 17:24:26 (UTC).
See https://pubs.acs.org/sharingguidelines for options on how to legitimately share published articles.

INTRODUCTION

Industrial processes that depend on conventional separation techniques account for almost 15% of global energy consumption,[1] which results in the emission of millions of tons of CO_2 annually. Separations based on adsorbents, including chromatography, will provide energy-efficient alternatives to these energy-intensive methods.[2−6] Novel adsorbents based on modular framework materials, such as metal−organic frameworks (MOFs) or covalent organic frameworks (COFs), are promising for energy-efficient separations because of their precise, nanoporous structures whose chemical functionality and voids can be tuned through judicious monomer selection.[7,8] Among framework materials, two-dimensional (2D) COFs are composed of layered 2D polymers (2DPs) that have shown promising thermal conductivity,[9−13] catalytic activity,[14−18] and stimuli-responsive changes relevant for sensors.[9,19−21] 2D COFs are also promising candidates for separations because their pore sizes, shapes, functionalities, and interlayer stacking arrangements can be tuned by modifying their building blocks.[22−25] However, most reported syntheses produce COFs as aggregates with nanometer-scale crystalline domains.[26−32] We recently reported a new method to grow imine-linked 2D COFs as suspensions of layered, faceted single-crystalline 2DP sheets by employing aniline as a chemical modulator and benzoic acid as a transimination catalyst.[33] 2D COF single crystals showed promise for an

Received: November 17, 2022
Revised: January 30, 2023

© XXXX American Chemical Society

energy-efficient gas chromatographic separation of benzene and cyclohexane, and polycrystalline COFs containing the same monomers showed no separation.[33]

In addition to being an important analytical technique, high-resolution gas chromatography provides insight into the material properties of a stationary phase by determining its physicochemical adsorption interactions with analytes of interest. Chromatographic separation allows for the rapid estimation of selectivity compared to other separation techniques such as crystallization,[34] distillation,[35] or membrane separation,[36] which require more extensive calibration and calculations.[37] Inverse pulse gas chromatography (IGC) is a method of conducting pressure-controlled gas chromatographic separations of standard probes at different temperatures to characterize the behavior of a novel stationary phase, in contrast to other quantitative and/or qualitative analyses of mixtures using an established stationary phase.[38] Here, we use IGC to quantitatively characterize the physiochemical adsorption properties and acid−base interactions of the adsorbent surface (represented by its electron donor−acceptor properties) of both single-crystalline and polycrystalline imine-linked 2D COFs. The difference in behavior of the COF samples in these experiments provides insight into the accessible surfaces, pores, and chemical functionalities found in both types of samples, despite their nearly identical chemical composition and similar bulk crystallinity. COFs are far less explored than MOFs[39−42] for chromatographic separation attempts,[43−47] and even fewer studies have used COFs for gas chromatography (GC).[48,49] Here, we use single-crystalline and polycrystalline samples of an imine-linked 2D COF (**TAPPy-PDA**) as GC stationary phases to separate both a series of linear alkanes and a series of standard polar probes. The McReynolds constants, which describe the polarity of the stationary phase, revealed that the single-crystalline **TAPPy-PDA** COF exhibits a nonpolar character, even less polar than that of common squalane stationary phases. In contrast, the polycrystalline **TAPPy-PDA** COF exhibited a slightly polar character. The study of the polar probes revealed that the single-crystalline **TAPPy-PDA** COF exhibits electron donor (Lewis basic) character, and the polycrystalline **TAPPy-PDA** COF instead exhibits electron acceptor (Lewis acidic) character. These findings indicate that the different COF crystals, which have identical chemical composition and similar bulk X-ray diffraction and spectroscopy, interact with analytes quite differently. We attribute these differences to the single-crystalline **TAPPy-PDA** COF interacting with analytes via its well-defined, square-shaped pores. The different behavior of polycrystalline **TAPPy-PDA** COF is attributed to analytes interacting to a greater extent with its outer surfaces and/or grain boundaries. These findings establish an approach to characterize the properties of 2D COFs for energy-efficient separations and demonstrate the importance of achieving high materials quality prior to establishing the relationship between COF structure and separation characteristics.

MATERIALS AND METHODS

COF monomers and reagents (1,3,6,8-tetrakis(4-aminophenyl)-pyrene), terephthalaldehyde, benzoic acid, aniline, and benzonitrile were purchased in reagent grade from commercial suppliers and used without further purification, unless otherwise described. High-purity air, helium, hydrogen, nitrogen, and methane gases (99.9999%) were supplied by SIGAS (Riyadh, Saudi Arabia). Linear alkanes series (pentane to octane) as well as acetonitrile (ACN), dichloromethane (DCM), diethyl ether (Et_2O), tetrahydrofuran (THF), and ethyl acetate (EtOAc), high-purity probes, were purchased from Merck (Darmstadt, Germany). Benzene, 1-butanol, 2-pentanone, 1-nitropropane, and pyridine were obtained from BDH (Lutterworth, U.K.).

Instrumentation. *Sonication.* Sonication was performed with a Branson 3510 ultrasonic cleaner with a power output of 100 W and a frequency of 42 kHz.

Centrifugation. Centrifugation was performed with a Fisherbrand Mini-Centrifuge operating at 6500 rpm.

Critical Point Drying. The supercritical CO_2 drying was performed on Leica EM CPD 300. Prior to the supercritical drying process, all samples were placed in tea bags (ETS Drawstring Tea Filters, sold by English Tea Store) while wet. The tea bags containing the samples were then placed in the drying chamber. The drying chamber was first sealed, cooled, and filled with liquid CO_2, and after 2 min, the samples were vented quickly. This fill−vent cycle was repeated 99 times, after which the temperature was raised to 40 °C resulting in a chamber pressure of around 1300 psi, which is well above the critical point of CO_2. The chamber was held above the critical point for 5 min, after which the CO_2 source was turned off, and the pressure was released over a period of 5 min.

Powder X-ray Diffraction (PXRD). PXRD patterns were obtained at room temperature on an STOE-STADIP powder diffractometer equipped with an asymmetric curved Germanium monochromator (Cu $K\alpha_1$ radiation, λ = 1.54056 Å) and one-dimensional silicon strip detector (MYTHEN2 1K from DECTRIS). The line-focused Cu X-ray tube was operated at 40 kV and 40 mA. The as-obtained powder samples were sandwiched between two acetate foils (polymer sample with neither Bragg reflections nor broad peaks above 2θ = 10°) mounted in flat plates with a disc opening diameter of 8 mm and measured in transmission geometry in a rotating holder. The patterns were recorded in the 2θ range of 0−32° for an overall exposure time of 24 min. The instrument was calibrated against a NIST Silicon standard (640d) prior to the measurement.

Gas Sorption Isotherms. Nitrogen uptake experiments were conducted on a Micromeritics ASAP 2420 Accelerated Surface Area and Porosity Analyzer using 15−50 mg of samples in dried and tared analysis tubes equipped with filler rods and capped with a Transeal. Samples were heated to 40 °C at a rate of 1 °C min^{-1} and evacuated at 40 °C for 20 min, then heated to 100 °C at a rate of 1 °C min^{-1} heat and evacuated at 100 °C for 18 h. After degassing, each tube was weighed again to determine the mass of the activated sample and transferred to the analysis port of the instrument. UHP-grade (99.999% purity) N_2 was used for all adsorption measurements. N_2 isotherms were generated by incremental exposure to nitrogen up to 760 mmHg (1 atm) in a liquid nitrogen (77 K) bath. Oil-free vacuum pumps and oil-free pressure regulators were used for all measurements. Brunauer−Emmett−Teller (BET) surface areas were calculated from the linear region of the N_2 isotherm at 77 K within the pressure range P/P_0 of 0.05−0.20. Pore size distributions were analyzed using nonlocal density functional theory (NLDFT) analysis on the MicroActive software using a model of N_2 at 77 K being adsorbed and desorbed into cylindrical pores of a porous oxide surface.

Fourier Transform Infrared (FT-IR) Spectroscopy. Infrared spectra were recorded using a Nicolet iS10 FT-IR spectrometer equipped with a Diamond ATR using solid COF powder after PXRD analysis and N_2 sorption measurements had been performed. Spectra were collected using 16 scans.

Nuclear Magnetic Resonance (NMR) Spectroscopy. Proton nuclear magnetic resonance (^{1}H NMR) spectra and carbon nuclear magnetic resonance (^{13}C NMR) spectra were recorded at 25 °C on a Bruker AvanceIII-500 MHz. The spectra were calibrated using residual solvent as internal reference ($CDCl_3$: 7.26 ppm for ^{1}H NMR, 77.00 for ^{13}C NMR).

Solid-State ^{13}C Cross-Polarization Magic Angle Spinning (CP-MAS) NMR Spectroscopy. Spectra were taken on a Varian 400 MHz with a spinning rate of 10 KHz. The spectra were recorded at 25 °C and referenced using adamantane/KBr as an external standard.

https://doi.org/10.1021/acs.chemmater.2c03448
Chem. Mater. XXXX, XXX, XXX−XXX

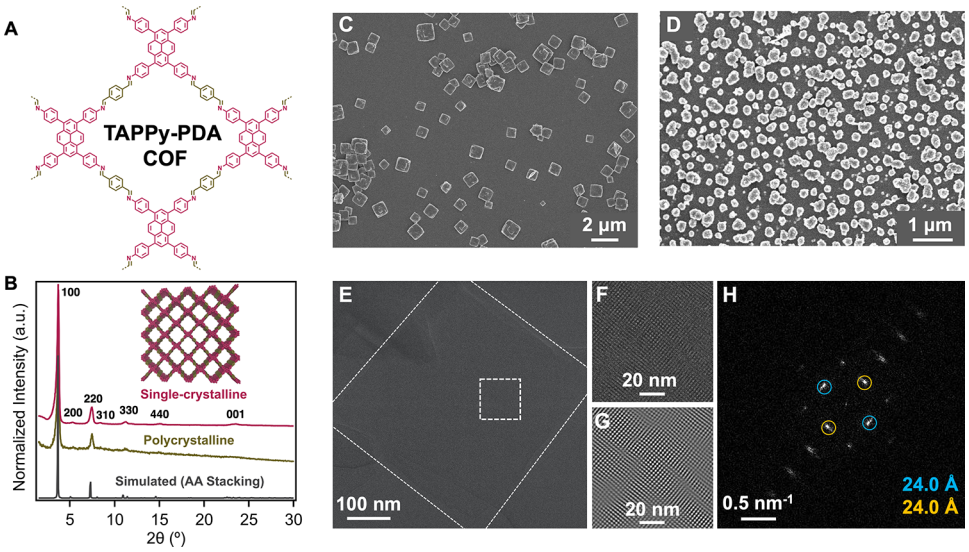

Figure 1. (A) Chemical structure and (B) experimental and simulated PXRD patterns of **TAPPy-PDA** COF. SEM images of (C) single-crystalline and (D) polycrystalline **TAPPy-PDA** COF. (E) Representative HRTEM image of a 1 μm sized COF single crystal with dashed lines drawn around the edges of the crystal as a guide to the eye. (F) Lattice-resolution HRTEM image of the boxed region in (E), and (G) a bandpass-filtered image of (F) with enhanced contrast. (H) Fast Fourier transform (FFT) of the boxed region in (E), with spots circled (blue, orange) that correspond to d_{100} spacings of 24.0 Å.

Ultraviolet–Visible (UV–Vis) Absorption Spectroscopy. UV–vis absorption spectra were acquired using a Cary 5000 UVVisNIR spectrophotometer equipped with a mercury lamp. All absorption spectra were recorded at room temperature in the presence of air. All samples were analyzed in 1 cm quartz cuvettes and were prepared from a 0.1 mg mL^{-1} solution of COF colloids in acetonitrile.

Scanning Electron Microscopy (SEM). SEM images of **TAPPy-PDA** and **TAPB-DMPDA** COFs were taken on a Hitachi S4800 cFEG SEM with an accelerating voltage of 15.0 kV. Prior to imaging, all samples were attached to flat aluminum stubs using double-sided tape and coated with 18 nm of osmium using an SPI OPC-60A Osmium Plasma Coater.

Atomic Force Microscopy (AFM). AFM images were collected using a Bruker Dimension Fastscan AFM in standard tapping mode. All samples were prepared from a 0.1 mg mL^{-1} solution of COF in benzonitrile.

High-Resolution Transmission Electron Microscopy (HRTEM). HRTEM imaging of the COF crystals was performed using a JEOL (JEOL USA, Inc., Peabody, MA) ARM300F GrandARM TEM operating at 300 keV equipped with a Gatan (Gatan, Inc., Pleasanton, CA) K3-IS "direct electron" detector (FEG Emission: 15 μA, spot size 5, 150 μm CL aperture). The ARM300F was aligned for low-dose imaging, measuring the dose rate on the K3 detector through vacuum (no grid inserted). The dose rate used was 0.61e$^-$ Å^{-2} s^{-1} for low-magnification images (5760 × 4092 pixels, binning 2), with an image exposure time of 1 s (0.61e$^-$ Å^{-2} cumulative dose per image). All image acquisition was done using the Gatan Microscopy Suite (GMS), Digital Micrograph (Gatan, Inc., Pleasanton, CA).

Gas Chromatography Capillary Coating. GC measurements were performed using a Shimadzu 2025 Series gas chromatograph equipped with a flame ionization detector (FID). Before dynamic coating, a fused silica capillary tubing (20 m long × 0.25 mm i.d.; CM Scientific, Silsden, United Kingdom) was pretreated by washing with 1 M NaOH for 2 h, ultrapure water for 30 min, 0.1 M HCl for 2 h, then ultrapure water until the pH was 7.0. Then, it was dried overnight under a constant flow of nitrogen at 423 K. Each batch of the pretreated capillaries was dynamically coated with either single-crystalline or polycrystalline **TAPPy-PDA** COFs.[50] To make a wet coating layer on the inner wall of the capillary column, a 1 mL suspension of either single-crystalline or polycrystalline **TAPPy-PDA** COF in ethanol (2 mg mL^{-1}) was first loaded into the column under nitrogen pressure and then forced out of the column at a velocity of 30 cm min^{-1}. A 1 m long buffer tube was added to the end of the capillary column as a restrictor to avoid solution acceleration. After coating, the capillary column was allowed to dry for 2 h under the same nitrogen flow. Finally, the capillary columns were preconditioned using the gas chromatograph with a temperature program starting at 303 K for 10 min, followed by a ramp from 303 to 573 K at a rate of 3 K min^{-1}, and a final equilibration step at 573 K for 30 min. After repeating the temperature program three times, the difference in masses of the coated capillary columns and the empty capillaries was used to estimate the mass of COF coating the insides of the columns.

Experimental Procedures.[33] *TAPPy-PDA Single-Crystalline COF (~1 μm).* A 40 mL scintillation vial was charged with benzoic acid (0.938 g, 7.68 mmol) and benzonitrile (3.56 mL). The vial was capped and heated to 90 °C until all of the benzoic acid had fully dissolved in solution. The vial was uncapped and a stock solution of terephthalaldehyde (**PDA**, (12 mg, 0.089 mmol) in 1 mL of benzonitrile) was added using a micropipette. Immediately after the addition of the **PDA** was added aniline (0.438 mL of a 0.70 M stock solution in benzonitrile, corresponding to 1.6 equiv. aniline per aldehyde functional group) using a micropipette. Finally, immediately after the addition of aniline, a stock solution of 1,3,6,8-tetrakis(4-aminophenyl)pyrene (**TAPPy** (28 mg, 0.050 mmol) in 1 mL of benzonitrile) was added to the reaction mixture. The scintillation vial was immediately capped without any shaking or stirring and held at 90 °C for 5 min, then cooled to room temperature until orange colloids were observed. Aliquots were taken from this reaction mixture and used for SEM, AFM, and HRTEM with 10-fold dilution in benzonitrile. The orange colloids were precipitated by the addition of 1 mL of brine and 10 mL of methanol, then centrifuged for 10 min to obtain the COF as a pellet. The COF pellet was then filtered into a tea bag and washed with methanol in a Soxhlet extractor for 18 h. The material was then activated in a supercritical CO_2 dryer to afford single-crystalline TAPPy-PDA COF as a yellow-orange solid in isolated yields of 80%.

TAPPy-PDA Polycrystalline COF. A 40 mL scintillation vial was charged with benzoic acid (0.228 g, 1.90 mmol) and terephthalaldehyde (**PDA**, 12 mg, 0.089 mmol) in benzonitrile (6 mL) and heated to 90 °C for a few minutes to ensure complete dissolution of each compound. To the solution were added, using a micropipette, water (0.120 mL, 33 equiv per aldehyde functional group), aniline (0.080 mL of 0.70 M stock in benzonitrile corresponding to 0.28 equiv per aldehyde functional group), and 1,3,6,8-tetrakis(4-aminophenyl)-

https://doi.org/10.1021/acs.chemmater.2c03448
Chem. Mater. XXXX, XXX, XXX−XXX

pyrene (**TAPPy**, 28 mg, 0.050 mmol). The scintillation vial was immediately capped without any shaking or stirring and held at 90 °C for 3 h, then cooled to room temperature until orange colloids were observed. Aliquots were taken from this reaction mixture and used for SEM with 10-fold dilution in benzonitrile. The orange colloids were precipitated by the addition of 2 mL of brine and 15 mL of methanol, then centrifuged for 10 min to obtain the COF as a pellet. The COF pellet was then filtered into a tea bag and washed with methanol in a Soxhlet extractor for 18 h. The material was then activated in a supercritical CO_2 dryer to afford polycrystalline **TAPPy-PDA** COF as a yellow-orange solid in isolated yields of 90%.

RESULTS AND DISCUSSION

Characterization of TAPPy-PDA COFs. Single-crystalline and polycrystalline **TAPPy-PDA** COFs (Figure 1A) were prepared from 1,3,6,8-tetrakis(4-aminophenyl)pyrene (**TAPPy**) and terephthalaldehyde (**PDA**) as stable colloids with lengths of ∼1 μm and ∼200 nm, respectively, using procedures that we recently reported.[33] Upon isolating and activating the COFs to their powder forms, the resulting powder X-ray diffraction (PXRD) patterns exhibited sharp, diagnostic 100 Bragg diffraction peaks at $2\theta = 3.68°$, and the single-crystalline COF also exhibited several higher-order diffraction peaks that were all consistent with previously reported powder patterns and averaged eclipsed AA stacking models of the COF, except for broadening of the 001 peak (Figure 1B). Low-dose high-resolution transmission electron microscopy (HRTEM) of the isolated and drop-cast single-crystalline **TAPPy-PDA** COF colloids confirmed that the square-shaped platelets had uniform fourfold symmetry (Figure 1E−H) consistent with their visualization by scanning electron microscopy (SEM) that showed faceted squares with side lengths of ∼1 μm (Figure 1C), while the polycrystalline counterpart consisted of aggregated, nonuniform particles ∼200 nm in diameter as seen by SEM (Figure 1D). The structure of the single-crystalline **TAPPy-PDA** COF is likely composed of single-crystalline domains in-plane with disorder in the stacking dimension, based on our prior continuous rotation electron diffraction (cRED) analysis.[33] Analysis of the N_2 adsorption isotherm of the single-crystalline **TAPPy-PDA** COF provided an accessible Brunauer−Emmett−Teller (BET) surface area of 2600 $m^2\ g^{-1}$ (Figure S4), from which nonlocalized density functional theory (NLDFT) analysis provided a pore width distribution centered at ∼22 Å (Figure S4), which is consistent with its theoretical pore size of 25 Å. In contrast, the polycrystalline **TAPPy-PDA** COF had a lower BET surface area of 1500 $m^2\ g^{-1}$ and a broader pore width distribution (Figure S4). Fourier transform infrared (FT-IR) spectroscopy, ^{13}C cross-polarization magic angle spinning nuclear magnetic resonance (CP-MAS NMR) spectroscopy, and ultraviolet−visible absorption (UV−vis) spectroscopy measurements of both single-crystalline and polycrystalline **TAPPy-PDA** COFs matched our previous reports (Figures S1−S3).[33,51] Both COF samples resisted thermal breakdown until temperatures of 500 °C and above, as seen in the thermogravimetric analysis (TGA) profiles of the two COFs (Figure 2). The first point of major loss occurred at around 500 °C in both COF samples, establishing this temperature as an upper limit for GC measurements. The maximum temperature tested in the GC experiments was 150 °C, which is well below this limit.

Physicochemical Investigation of Adsorption. Initial inverse pulse gas chromatography (IGC) experiments suggested an exothermic adsorption process on the surfaces of both single-crystalline and polycrystalline **TAPPy-PDA** COFs. The IGC study provided physicochemical parameters to describe the interactions of single-crystalline and polycrystalline **TAPPy-PDA** COFs with a series of linear alkanes (pentane, hexane, heptane, and octane) as well as several polar probes such as acetonitrile (ACN), dichloromethane (DCM), diethyl ether (Et_2O), tetrahydrofuran (THF) and ethyl acetate (EtOAc; Table 1). Negative Gibbs free energy ΔG_A values (Table 1) indicated spontaneous transfer of solutes from the mobile to the stationary phase. Furthermore, the adsorption enthalpies (ΔH_A; Table 1) did not exceed the physical−chemical adsorption threshold of 62.8 kJ mol^{-1},[52] indicating that all testing probes solely interacted physically with the single-crystalline and polycrystalline **TAPPy-PDA** COFs. The adsorption enthalpies (ΔH_A) over both single-crystalline and polycrystalline COF-coated columns were slightly greater than the corresponding liquefaction enthalpies (ΔH_{liq}; Table 1),[53] suggesting that adsorbate-adsorbent interactions dominated adsorbate-adsorbate interactions. The Van't Hoff plots of each probe in the series exhibited linear correlations, indicating that the interaction mechanism between the analyte and COF pores did not change during the separation process (Figures S5−S8). Furthermore, the slight difference in magnitude between the values of ΔH_A and ΔH_{liq} for each probe showed that secondary weak intermolecular forces or Liftshitz-van der Waals forces were responsible for most interactions across the surface. The linear dependency of the natural logarithm of the specific retention volume ($\ln V_g$) on the inverse temperature ($1/T$) implied a constant value of ΔH_A in the temperature range investigated (393−423 K; Figures S9−S12 and Table 1), indicating that both COF samples had an exothermic adsorption process across the temperature range investigated. Furthermore, the significant decline in the adjusted retention time of analytes with increasing the column temperature (Table S2) also confirmed an exothermic adsorption process in both COF samples, indicating that the surfaces of both single-crystalline and polycrystalline **TAPPy-PDA** COFs are energetically homogeneous toward the adsorption of the analytes tested. These observations indicate that COFs of the same chemical composition have similar surface interactions with analytes, yet the crystallinity and long-range order of the single-crystalline COFs dramatically influence the interactions of the analytes with their accessible surfaces.

The retention volume (V_N) of the linear alkanes increased with an increase in their chain length because of greater

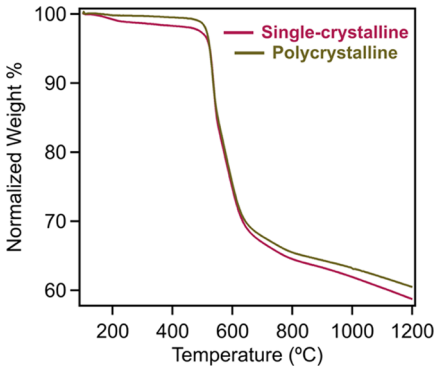

Figure 2. TGA profiles of single-crystalline (red trace) and polycrystalline (green trace) indicate that **TAPPy-PDA** COFs do not decompose to volatile byproducts until temperatures well above 300 °C.

https://doi.org/10.1021/acs.chemmater.2c03448
Chem. Mater. XXXX, XXX, XXX−XXX

Table 1. Gibbs Free Energy (ΔG_A) and Entropy (ΔS_A) of Adsorption at 423 K, Enthalpy of Adsorption (ΔH_A) in the Range 423−393 K, and Enthalpy of Liquefaction (ΔH_{liq}) of All Probes Tested on Columns Coated with Single-Crystalline and Polycrystalline TAPPy-PDA COFs at a Pressure of 0.2 MPa

	$-\Delta G_A$ (kJ mol^{-1})		$-\Delta S_A$ (J mol^{-1} K^{-1})		$-\Delta H_A$ (kJ mol^{-1})		
probe	single-crystalline	polycrystalline	single-crystalline	polycrystalline	single-crystalline	polycrystalline	$-\Delta H_{liq}$ (kJ mol^{-1})
pentane	24.4	25.9	44.7	58.1	43.3	50.5	26.4
hexane	25.1	27.0	60.9	81.0	50.9	61.3	31.6
heptane	25.9	28.3	77.3	104.6	58.6	72.6	36.6
octane	26.9	29.9	97.1	130.7	68.0	85.2	41.5
ACN	17.6	21.4	35.3	53.5	32.5	44.0	29.8
DCM	21.9	24.0	28.2	29.2	33.8	36.4	28.1
Et_2O	24.5	26.5	33.4	49.6	38.6	47.5	27.1
THF	22.9	25.0	41.9	52.2	40.6	47.1	29.6
EtOAc	23.4	26.4	48.5	63.1	43.9	53.1	35.6

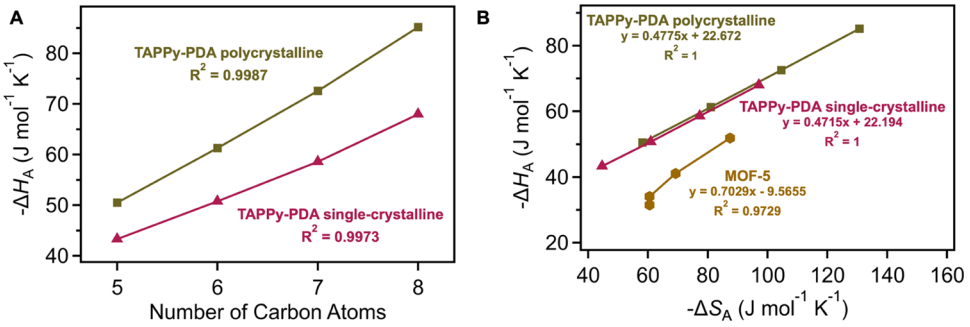

Figure 3. (A) Effects of the alkyl chain length on enthalpy of adsorption, ΔH_A, in the temperature range 423−393 K. (B) Thermodynamic compensation effect between entropy of adsorption, ΔS_A, at 423 K and enthalpy of adsorption, ΔH_A, in the temperature range 423−393 K, for *n*-alkanes (pentane, hexane, heptane, and octane) on single-crystalline and polycrystalline **TAPPy-PDA** COFs and on **MOF-5**.[55] Data recorded at 0.2 MPa.

reduction in vapor pressure in longer-chain molecules (Table S3).[49] Furthermore, due to the additive nature of dispersive interactions, a linear relationship was observed between the adsorption enthalpy (ΔH_A) and the chain length of *n*-alkanes (Figure 3A).[54] ΔH_A values for the linear alkanes were more negative on the columns coated with polycrystalline **TAPPy-PDA** than those coated with single-crystalline **TAPPy-PDA** (Figure 3B). It is possible that the polycrystalline **TAPPy-PDA** COF is composed of less well-defined surface states and grain boundaries, creating more adsorption active sites in the COF pores and therefore resulting in stronger adsorption interactions than those observed in single crystals of **TAPPy-PDA**. Both COF samples showed more negative ΔH_A values than the archetypal metal−organic framework **MOF-5**, which was used as a reference framework material for comparison (Figure 3B).[55] Similarly, the adsorption entropy (ΔS_A) values of all alkanes measured, except pentane,[56] were greater in columns coated with either sample of **TAPPy-PDA** sample compared to the column coated with **MOF-5**. Given that the adsorption entropy (ΔS_A) measures the loss of freedom in adsorbates, typically, immobilizing an adsorbate reduces the amount of disorder in the adsorbate-adsorbent interactions. The higher magnitude ΔS_A values in both **TAPPy-PDA** COF samples indicated a greater retention of adsorbate probes and a more restricted movement of the adsorbates down the column.[56] With correlation coefficients of 1 for both COFs studied, Figure 3B depicts a perfect linear relationship between ΔH_A and ΔS_A for all alkanes tested on columns coated with either COF sample, illustrating the thermodynamic compensation effect. The linearity in the relationship between adsorption enthalpies and entropies indicated that nonspecific interactions were predominant and that the longer *n*-alkanes are adsorbed into the COF pores with a lower degree of freedom and hence likely a stronger interaction with the COF surface.[57] Since the slope of compensation of the linear correlation is considered a process characteristic, the difference in the magnitude of the slopes obtained for **TAPPy-PDA** COFs and **MOF-5** suggested distinct equilibrium processes and different modes of interaction (Figure 3B), while similar slopes for single-crystalline and polycrystalline **TAPPy-PDA** COFs denoted a similar nature of the interaction of the *n*-alkanes with both COFs.[58] Thus, the **TAPPy-PDA** COFs, regardless of their materials quality, likely have an overall less disordered adsorption system and therefore greater potential for high-efficiency separations of small molecules compared to **MOF-5**.

The chromatographic resolution (R_S) of the *n*-alkanes, which defines the degree of separation between two successive peaks on a chromatogram, showed the greatest sensitivity to COF materials quality. This parameter describes both the selectivity and efficiency of the separation. R_S was calculated from the ratio of the distance between two successive peaks and the average width of these peaks, and an R_S value greater than 1.2 is required to conclude that complete separation has occurred. R_S was calculated for *n*-alkanes at 423 K to demonstrate the effect of the degree of crystallinity of COF materials on separation. The column coated with single-crystalline **TAPPy-PDA** exhibited a higher resolution of separation of *n*-alkane pairs (eq S1), pentane/hexane (1.47), hexane/heptane (3.4), and heptane/octane (7.35), in contrast to the column coated with polycrystalline **TAPPy-PDA**, which

https://doi.org/10.1021/acs.chemmater.2c03448
Chem. Mater. XXXX, XXX, XXX−XXX

showed lower resolution with values of 0.64, 0.98 and 1.28 for pentane/hexane, hexane/heptane and heptane/octane, respectively. Therefore, despite the higher adsorption enthalpy and Gibbs free energy values of the polycrystalline COF surface, the single-crystalline COF provides better separation and superior resolution of these analytes, which we attribute to its high crystallinity and well-defined pores.

Estimation of the Dispersive Component of Surface Energy. The surface interaction of linear alkanes was also investigated in terms of the dispersive component of the surface energy of the adsorbent (γ_S^D).[59] The dispersive component is related to London forces and analogous to surface tension in liquids. This parameter is marginally more sensitive to surface variations than the enthalpy of adsorption (ΔH_A). The methods reported by Dorris and Gray[60] as well as Schultz et al.[61] were used to determine the values of γ_S^D (Table 2). The Dorris−Gray dispersive component of surface energy

Table 2. Summary of the Dispersive Component of Surface Energy γ_S^D (mJ m^{-2}) Values Calculated Using the Dorris−Gray and Schultz et al. Methods for Single-Crystalline and Polycrystalline TAPPy-PDA COFs in the Temperature Range of 423−393 K at a Pressure of 0.2 MPa

	γ_S^D, Dorris−Gray method (mJ m^{-2})		γ_S^D, Schultz et al. method (mJ m^{-2})	
T (K)	single-crystalline	polycrystalline	single-crystalline	polycrystalline
423	82.9	108.3	56.8	74.6
413	85.4	121.8	59.9	84.9
403	89.6	124.3	64.2	89.6
393	94.5	134.8	68.9	99.3

values for the single-crystalline and polycrystalline COFs are in the same ranges as those reported for several typical MOFs such as **MOF-5** [(86 mJ m^{-2})[54] and (67 mJ m^{-2})[55]] and **HKUST-1**, **ZIF-8**, **Fe-BTC**, and **MIL-35** (107, 58, 54, and 51 mJ m^{-2}, respectively)[62] at 423 K. These values are significantly lower than those calculated via IGC for activated carbons, zeolites, and other microporous materials, which have reported values between 200 and 500 mJ m^{-2}.[63] **TAPPy-PDA** COFs have a larger pore size than many other microporous materials typically characterized by IGC, which may explain why these COFs have much lower values for the dispersive component of surface energy.[54] Generally, the dispersive component of surface free energy is inversely proportional to temperature due to the entropic component of surface energy. The dispersive parameters calculated using the Dorris−Gray approach were higher than those using the Schultz et al. method, as is commonly observed in adsorbent materials[64] (Table 2). Similarly, it is possible that the less well-defined surface states and grain boundaries found in polycrystalline **TAPPy-PDA** result in higher surface energy since the polycrystalline **TAPPy-PDA** COF has lower γ_S^D values than the single-crystalline **TAPPy-PDA** COF.

Determination of McReynolds Constants. The polarity of the stationary phase significantly impacts its separation selectivity. Early efforts to establish the selectivity scale were based on Rohrschneider's system of characteristic phase constants,[65,66] which was later updated by McReynolds.[66] Benzene, 1-butanol, 2-pentanone, 1-nitropropane, and pyridine were used to calculate McReynolds constants to describe the polarity of adsorption into single-crystalline and polycrystalline **TAPPy-PDA** COFs since each probe represents a specific type of interaction between the test molecule and the examined phase. Single-crystalline **TAPPy-PDA** was classified as a nonpolar stationary phase because it had an even smaller average value of the five McReynolds constants than the nonpolar standards squalane and single-walled carbon nanotubes (SWNT; Table 3). To our knowledge, single-crystalline **TAPPy-PDA** is the first COF material to exhibit such an extremely nonpolar character. The **cTpBD** COF reported by Yan and co-workers in 2016 is the closest in polarity to the single-crystalline **TAPPy-PDA**, and this adsorbent was classified as a moderate polarity material based on its McReynolds constants.[67] Among MOFs, the nonpolar **MOF-5** shows identical polarity to the single-crystalline **TAPPy-PDA** (Table 3).[68] In contrast, the polycrystalline **TAPPy-PDA** exhibits a weakly polar nature, with higher McReynolds constants than those of single-crystalline **TAPPy-PDA**.

The average of the McReynolds constants characterizes the relative polarity of materials in terms of their most effective adsorption active sites; however, it is not an absolute measure of a material's polarity. Each McReynolds probe is also an indicator of a specific molecular interaction. Both COFs have similar dispersion forces and polarizability, as indicated by the X' component that describes their interaction with the benzene. Single-crystalline **TAPPy-PDA** has a stronger hydrogen bonding ability, as demonstrated by the Y' component that

Table 3. McReynolds Constants for Single- and Polycrystalline TAPPy-PDA COFs Compared to Literature Values for Other Materials[a]

stationary phase	X'	Y'	Z'	U'	S'	average
ΔI squalane	0	0	0	0	0	0
ΔI **TAPPy-PDA** single-crystalline	−87.9	19.9	16.3	−28.5	−49.4	−25.9
ΔI **TAPPy-PDA** polycrystalline	−82.1	−19.5	50.0	3.0	311.6	52.6
ΔI CTpBD[67]	24.9	189	94.7	115	85.6	102
ΔI MOF-5[68]	−101	−33.0	1.00	−28.0	−23.0	−37.0
ΔI MIL-100(Fe)[69]	−45.8	−2.60	56.4	27.0	−105	−13.9
ΔI MIL-100(Cr)[69]	−32.5	97.9	44.6	43.7	−42.1	22.3
ΔI ZIF-90[70]	−67.0	19.0	83.0	51.0	41.0	25.4
ΔI KAPs-1[71]	−51.0	32.0	51.0	36.0	3.00	14.0
ΔI HP-5MS[71]	31.0	68.0	62.0	95.0	63.0	64.0
ΔI SWNT[72]	−63.0	100	125		176	

[a]Measured at 393 K; X', Y', Z', U', and S' represent interactions of the stationary phase with benzene,1-butanol, 2-pentanone, 1-nitropropane, and pyridine, respectively. The average describes the overall relative polarity of the material.

https://doi.org/10.1021/acs.chemmater.2c03448
Chem. Mater. XXXX, XXX, XXX−XXX

describes its interaction with *n*-butanol. Further, single-crystalline **TAPPy-PDA** also has a lower proton donor tendency as seen by the *Z*' term describing its interaction with 2-pentanone. Meanwhile, polycrystalline **TAPPy-PDA** has a stronger proton donor character as indicated by its strong retention of pyridine (*S*' term) which eluted between *n*-nonane and *n*-decane, unlike in single-crystalline **TAPPy-PDA** where it eluted between *n*-hexane and *n*-heptane. Dipole-dipole interactions, represented by the *U*' term describing interaction with nitropropane, are higher in polycrystalline **TAPPy-PDA**. Taken together, the McReynolds constants suggest that the single-crystalline **TAPPy-PDA** COF is more basic and has a stronger proton-accepting nature, while the polycrystalline **TAPPy-PDA** COF has a greater dipolar character and stronger ability to interact with proton-accepting solutes.

Calculation of Specific Interactions. Dispersive interactions (London forces) in *n*-alkane adsorption provide information on carbon structure, whereas specific interactions of the COF surface are determined using standard organic polar probes. In addition to dispersive interactions, the adsorption of polar molecules on the stationary phase involves specific components pertaining to various forms of van der Waals' forces, such as the Keesom orientation force and Debye inductive force, as well as hydrogen bonding, $\pi-\pi$ interactions and other noncovalent attractions.[73] The column coated with single-crystalline **TAPPy-PDA** showed rapid separation of the studied mixture of polar organic probes (ACN, DCM, Et_2O, THF, and EtOAc) in ~50 s in real time, equivalent to ~11 s in adjusted retention (Figure 4 and eq S2). The elution of these

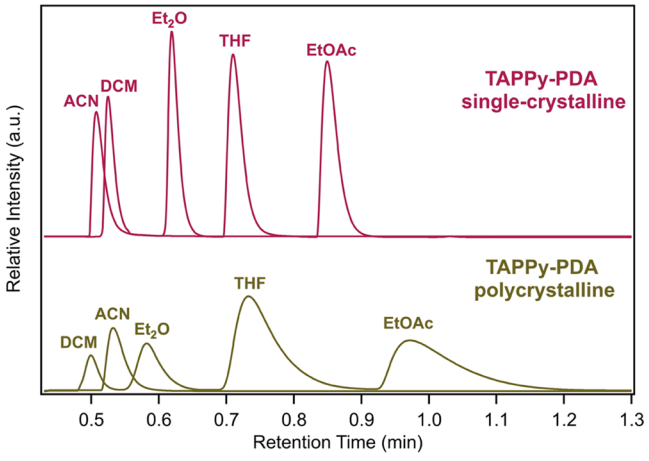

Figure 4. Gas chromatogram showing the separation of acetonitrile (ACN), dichloromethane (DCM), diethyl ether (Et_2O), tetrahydrofuran (THF), and ethyl acetate (EtOAc) on columns (20 m length × 0.25 mm i.d.) coated with single-crystalline and polycrystalline **TAPPy-PDA** COFs at a temperature of 393 K and a pressure of 0.2 MPa. Note: ACN was injected separately.

polar probes from the single-crystalline **TAPPy-PDA** COF-coated column followed the order: ACN, DCM, Et_2O, THF, and EtOAc. A different order of elution was observed for the column coated with polycrystalline **TAPPy-PDA**, with DCM eluting before ACN. This change indicates the different nature of interactions in the two COF materials. The order of the retention times of the analytes would reflect the order of their boiling points if the separation process were mostly controlled by London dispersive interactions; however, this is not the case in either COF material given that the isothermal separation temperature (393 K) was much higher than the boiling points of any of the polar probes (Table S1). The probe with the highest boiling point (ACN; b.p. = 81.6 °C) eluted first in the column coated with single-crystalline **TAPPy-PDA** but eluted second in the column coated with polycrystalline **TAPPy-PDA**. Taken together, it seems that the boiling points have a minor effect on separation and that the main driving force for separation lies in the interaction of analytes with the stationary phase.

The specific free energy of adsorption (ΔG^S), which reports the overall interactions of analytes with the stationary phase, is calculated by subtracting the free energy of adsorption of a hypothetical or real linear alkane (ΔG_{ref}) from the free energy of adsorption of a polar analyte (ΔG_A) (eq S12). The reference linear alkane must have some allocated property similar to that of a polar probe, such as vapor pressure given by the Papirer et al. method,[74] dispersive free energy $(\gamma_L^D)^{1/2}$ of solute given by the Schultz–Lavielle methods,[60,61] or polarizability of probes (α_o) given by the Donnet et al. method.[75] The validity of all three methods was investigated to estimate the specific free energy of adsorption (ΔG^S) of each alkane.

As expected, the Papirer et al. and Schultz–Lavielle methods failed to estimate the ΔG^S of both COFs studied. Representative points for polar probes were found below the reference line for *n*-alkanes using both methods (Figures S13–S16). Although these methods have been successful for many solid surfaces, they usually fail to describe materials with high London dispersive force components.[75] The liquid state used as a reference in the prior techniques operates in a state that is significantly different from the adsorbate-adsorbent interaction that occurs between discrete molecules and the studied material surfaces at infinite dilution conditions. Furthermore, in characterizing solid materials with high London dispersive surface energy, measurements must be conducted at ~423 K, a temperature that is higher than the room temperature condition at which $(\gamma_L^D)^{1/2}$ and the molecular surface area (α) are measured based on Schultz–Lavielle method. On the other hand, the polarizabilities of the test probes were more accurate in estimating ΔG^S using the Donnet et al. approach (Figures S17–S18). Though these contrasting results are perhaps unsurprising to those familiar with these calculations, these comparisons have not been previously done for COFs or MOFs with the goal of identifying the best approach to address the adsorption-specific contribution of surface energy for crystalline organic framework materials.

The parameter of specific interaction, I^{sp}, is directly related to the polarity of the adsorbate and was calculated from the ΔG^S of the adsorbate by taking into account the molecular surface area of the polar probe[55] (Table 4). Based on I^{sp} calculations, ACN exhibited the largest specific interaction with the studied COF materials. This behavior can be explained by the presence of the π-electron-rich triple bond that could enhance $\pi-\pi$ interactions with the framework in addition to the sterically accessible nonbonding electrons on the nitrogen atom. Therefore, the weakest retention of ACN on the nonpolar surface of the single-crystalline **TAPPy-PDA** COF, and therefore the corresponding lowest ΔH_A value, could be attributed to the fact that ACN is more polar than the other probes. DCM, which has Lewis acidic character based on its Gutman's electron donor number (DN = 0), and its Riddle–Fowkes' electron acceptor number (AN* = 16.3; Table S1), is retained to a greater extent on the column coated with single-crystalline **TAPPy-PDA**, which has a less acidic

https://doi.org/10.1021/acs.chemmater.2c03448
Chem. Mater. XXXX, XXX, XXX–XXX

Table 4. Specific Free Energies of Adsorption (ΔG^S) and Specific Components of Adsorption Energies (I^{sp}) of Polar Probes on Columns Coated with Single-Crystalline and Polycrystalline TAPPy-PDA COFs at a Temperature of 423 K and a Pressure of 0.2 MPa

	$-\Delta G^S$ (kJ mol^{-1})		$-I^{sp}$ (mJ m^{-2})	
probe	single-crystalline	polycrystalline	single-crystalline	polycrystalline
ACN	6.3	10.2	48.5	78.9
DCM	3.5	5.6	18.4	29.5
Et_2O	1.9	2.8	6.70	9.80
THF	4.6	5.8	17.1	21.4
EtOAc	2.5	4.1	8.60	14.3

character as estimated by McReynolds constants. The reversed elution order between ACN and DCM on single-crystalline **TAPPy-PDA** was reasonable since the McReynolds study revealed single-crystalline **TAPPy-PDA** to be less polar and more acidic than its polycrystalline counterpart. Et_2O had the lowest I^{sp} values, likely due to the ethyl groups shielding the oxygen atom and reducing its access to the COF pores. In contrast, the I^{sp} values of THF were much higher due to the exposed oxygen atom, supporting the structural effect observation. The very low boiling point of Et_2O could also explain its relatively short elution time in spite of its nonpolar behavior (especially on single-crystalline **TAPPy-PDA**) predicting longer elution times.

Determination of Electron Donor−Acceptor Character. To better understand the electron donor−acceptor properties of the COFs, the specific enthalpies of adsorption (ΔH^S) of the surfaces of both COFs were determined from the slope of $\Delta G^S/T$ plotted as a function of $1/T$ (Figures S19 and S20). The ΔH^S values were then used to estimate the Lewis acid−base properties using eq S15. The linear relation of ΔH^S/AN* vs DN/AN* (DN: Gutman's electron donor number, and AN*: Riddle−Fowkes' electron acceptor number) was used to calculate the electron acceptor constant (K_A) from the slope and the electron donor constant (K_B) from the intercept (Figure 5). The surfaces of single-crystalline and polycrystalline **TAPPy-PDA**, the acidic character could be attributed to the dominating interactions with the external surface states, which might have more Lewis acidic groups (such as dangling aldehydes). Taken together, the electron donor character of single-crystalline **TAPPy-PDA** likely originates from its high crystallinity and well-defined pore channels, amplifying the effect of mildly basic imines lining the insides of the COF channels. Meanwhile, we speculate that the electron acceptor character of polycrystalline **TAPPy-PDA** arises from its lower crystallinity and limited long-range order, which causes the adsorbates to interact to a greater extent with its surface.

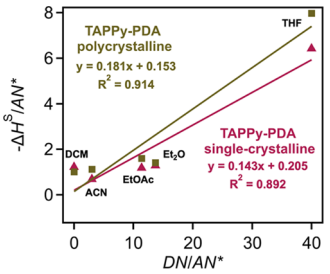

Figure 5. Plot of $-\Delta H^S$/AN* vs DN/AN* for the adsorption of polar probes on columns coated with single-crystalline and polycrystalline **TAPPy-PDA** COFs in the temperature range of 423−393 K and at a pressure of 0.2 MPa. Each line is a linear fit with the equations and square of the correlation coefficients given on the plot.

line **TAPPy-PDA** COFs had K_A values of 0.14 and 0.18, respectively, and K_B values of 0.21 and 0.15, respectively, suggesting that the single-crystalline **TAPPy-PDA** had a Lewis basic character with $K_B/K_A > 1$. In contrast, the polycrystalline **TAPPy-PDA** had a Lewis acidic character with $K_B/K_A < 1$, consistent with the results of the McReynolds constants study and polar probes retention study. The mildly basic character of single-crystalline **TAPPy-PDA** could be attributed to the Lewis basic N atoms in imine bonds within channels. For

Evaluation of COF-Containing GC Columns after Aging for 18 Months. Structural and performance characterization of COF samples aged for 18 months under ambient conditions indicated that single-crystalline **TAPPy-PDA** COFs are more stable than polycrystalline **TAPPy-PDA** COFs. Gas chromatography experiments were repeated on columns aged 18 months using three linear alkane probes (pentane, hexane, and heptane). The gas chromatography experiments indicated that ΔS_A was more strongly affected by aging than ΔH_A for both the single-crystalline and polycrystalline samples. ΔS_A decreased by 12.6 and 15.6% for single-crystalline **TAPPy-PDA** COFs and polycrystalline **TAPPy-PDA** COFs, respectively, whereas ΔH_A decreased by 7.0 and 4.4% for single-crystalline **TAPPy-PDA** COFs and polycrystalline **TAPPy-PDA** COFs, respectively (Table S11). The more significant decrease in entropy than enthalpy in both materials results from the decline in surface area, which affects entropy but has no direct effect on enthalpy. The average values of dispersive component of surface energy values for single-crystalline and polycrystalline **TAPPy-PDA** COFs were decreased by 11 and 2%, respectively (Table S12). The dispersive component of surface energy is more sensitive to surface variations than ΔH_A such that changes associated with the well-defined, crystalline structure of single-crystalline **TAPPy-PDA** COFs will be more easily measured than changes to the polycrystalline **TAPPy-PDA** COFs. The McReynolds constant of the single-crystalline **TAPPy-PDA** COF was almost unchanged after 18 months, with only a slight increase in polarity (Table S13). The polycrystalline **TAPPy-PDA** COFs showed sharp variations in their McReynolds constants and the average value, indicating a significant change in the functional adsorption sites over time. Over the same aging period, S_{BET} of bulk samples of single-crystalline **TAPPy-PDA** decreased by 16.9%, from 2600 to 2160 m^2 g^{-1}, and S_{BET} of the polycrystalline **TAPPy-PDA** decreased by 52%, from 1500 to 720 m^2 g^{-1}. Taken together, these extensive measurements of samples aged for 18 months indicate promise for the single-crystalline samples to be sufficiently stable for long-term use, and their stability might

https://doi.org/10.1021/acs.chemmater.2c03448
Chem. Mater. XXXX, XXX, XXX−XXX

improve further following the development of appropriate storage protocols.

CONCLUSIONS

IGC was used to quantify electron donor−acceptor properties, physiochemical parameters, polarities, and acid−base properties of single-crystalline and polycrystalline samples of an imine-linked 2D COF (**TAPPy-PDA**). A series of linear alkanes and a mixture of polar probes were separated at moderate pressure and temperatures ranging from 393 to 423 K over open-tubular GC columns coated with either sample of the **TAPPy-PDA** COF as a stationary phase.

The IGC studies characterized the single-crystalline **TAPPy-PDA** as a nonpolar adsorbent with electron-donating (Lewis basic) character and the polycrystalline **TAPPy-PDA** as a more polar adsorbent with electron-accepting (Lewis acidic) character. These differences are striking given that both materials are based on the same monomers and have similar rhombic topologies. An investigation of the commonly used methods to study specific free energies of adsorption (ΔG^S) revealed that the Papirer et al. and the Schultz and Lavielle methods are not suitable for 2D COFs, whereas the Donnet et al. method based on the polarizability of the probes is the most appropriate method. Adsorption enthalpy (ΔH_A) calculations supported by the study of the dispersive component of surface energy revealed that both COF samples exhibited exothermic adsorption processes. However, polycrystalline **TAPPy-PDA** had a higher energy surface than single-crystalline **TAPPy-PDA**, likely due to its less well-defined surface states and grain boundaries. Single-crystalline **TAPPy-PDA** showed higher resolution and selectivity in its separation performance, likely due to improved long-range order and crystallinity. Furthermore, single-crystalline **TAPPy-PDA** was found to have a highly nonpolar character, and polycrystalline **TAPPy-PDA** a moderately polar character as characterized by their McReynolds constants. The nonpolar nature of single-crystalline **TAPPy-PDA** COF allows it to be regenerated after separation, which is ideal for both separation and catalytic adsorption applications. IGC allows precise and rapid characterization and comparison of porous materials, it has not yet been applied broadly for characterizing MOFs and especially 2D COFs.

The hydrophobic pores, high crystallinity, uniform, faceted morphology, high thermal stability, and high accessible surface area of the single-crystalline **TAPPy-PDA** COF also make it a promising candidate for other adsorbent-based separations such as reverse-phase high-performance liquid chromatography (RP-HPLC). Most notably, the findings of this manuscript consistently indicate that polycrystalline COFs, in addition to showing inferior separation performance, also show completely different adsorbent properties compared to single-crystalline COFs. Therefore, synthesizing high-quality, ideally single-crystalline, COFs and implementing them in adsorbent-based separations is a prerequisite to develop reliable connections between COF structure and performance, a long-sought promise of this emerging polymer architecture.

ASSOCIATED CONTENT

Supporting Information

The Supporting Information is available free of charge at https://pubs.acs.org/doi/10.1021/acs.chemmater.2c03448.

Materials and instrumentation, experimental procedures, additional COF characterization, chromatographic setup, and IGC calculations (PDF)

AUTHOR INFORMATION

Corresponding Authors

Kareem Yusuf − *Department of Chemistry, College of Science, King Saud University, Riyadh 11451, Saudi Arabia;* orcid.org/0000-0002-7127-8750; Email: kmahmoud@ksu.edu.sa

William R. Dichtel − *Department of Chemistry, Northwestern University, Evanston, Illinois 60208, United States;* orcid.org/0000-0002-3635-6119; Email: wdichtel@northwestern.edu

Authors

Anusree Natraj − *Department of Chemistry, Northwestern University, Evanston, Illinois 60208, United States;* orcid.org/0000-0003-4171-9815

Kelvin Li − *Department of Chemistry, Northwestern University, Evanston, Illinois 60208, United States*

Mohamed Ateia − *Department of Chemistry, Northwestern University, Evanston, Illinois 60208, United States;* Present Address: M.A.: Center for Environmental Solutions and Emergency Response, United States Environmental Protection Agency, Cincinnati, Ohio 45220, United States; orcid.org/0000-0002-3524-5513

Zeid A. ALOthman − *Department of Chemistry, College of Science, King Saud University, Riyadh 11451, Saudi Arabia;* orcid.org/0000-0001-9970-2480

Complete contact information is available at: https://pubs.acs.org/10.1021/acs.chemmater.2c03448

Author Contributions

[§]K.Y. and A.N. contributed equally to this work.

Notes

The authors declare no competing financial interest.

ACKNOWLEDGMENTS

The authors thank Dr. Ioannina Castano for acquiring TEM images of the COF samples. They acknowledge the Army Research Office (ARO) for a Multidisciplinary University Research Initiatives (MURI) award under Grant Number (W911NF-15-1-0447) awarded to W.R.D. This work has made use of the Integrated Molecular and Structure Education and Research Center (IMSERC) at Northwestern University, which has received support from the National Science Foundation (NSF) through Grant Number (CHE-1048773). This work has also made use of the Electron Probe Instrumentation Center (EPIC) and Keck II facilities of the Northwestern University Atomic and Nanoscale Characterization Experiment (NUANCE) Center, which has received support from the Soft and Hybrid Nanotechnology Experimental (SHyNE) Resource (NSF; ECCS-1542205), the MRSEC program (NSF; DMR-1720139) at the Materials Research Center, the Keck Foundation, the State of Illinois, and the International Institute for Nanotechnology (IIN). A.N. was supported by the Ryan Fellowship and IIN. This work was also funded by the Researchers Supporting Project Number (RSP2022R429) through King Saud University, Riyadh, Saudi Arabia.

REFERENCES

(1) Sholl, D. S.; Lively, R. P. Seven Chemical Separations to Change the World. *Nature* **2016**, *532*, 435−437.

(2) Li, X.; Liu, Y.; Wang, J.; Gascon, J.; Li, J.; Bruggen, B. V. der. Metal−Organic Frameworks Based Membranes for Liquid Separation. *Chem. Soc. Rev.* **2017**, *46*, 7124−7144.

(3) Shekhah, O.; Chernikova, V.; Belmabkhout, Y.; Eddaoudi, M. Metal−Organic Framework Membranes: From Fabrication to Gas Separation. *Crystals* **2018**, *8*, No. 412.

(4) Yuan, S.; Li, X.; Zhu, J.; Zhang, G.; Van Puyvelde, P.; Van der Bruggen, B. Covalent Organic Frameworks for Membrane Separation. *Chem. Soc. Rev.* **2019**, *48*, 2665−2681.

(5) Monjezi, B. H.; Kutonova, K.; Tsotsalas, M.; Henke, S.; Knebel, A. Current Trends in Metal−Organic and Covalent Organic Framework Membrane Materials. *Angew. Chem., Int. Ed.* **2021**, *60*, 15153−15164.

(6) Mukherjee, S.; Sensharma, D.; Qazvini, O. T.; Dutta, S.; Macreadie, L. K.; Ghosh, S. K.; Babarao, R. Advances in Adsorptive Separation of Benzene and Cyclohexane by Metal-Organic Framework Adsorbents. *Coord. Chem. Rev.* **2021**, *437*, No. 213852.

(7) Freund, R.; Zaremba, O.; Arnauts, G.; Ameloot, R.; Skorupskii, G.; Dincă, M.; Bavykina, A.; Gascon, J.; Ejsmont, A.; Goscianska, J.; Kalmutzki, M.; Lächelt, U.; Ploetz, E.; Diercks, C. S.; Wuttke, S. The Current Status of MOF and COF Applications. *Angew. Chem., Int. Ed.* **2021**, *60*, 23975−24001.

(8) Freund, R.; Canossa, S.; Cohen, S. M.; Yan, W.; Deng, H.; Guillerm, V.; Eddaoudi, M.; Madden, D. G.; Fairen-Jimenez, D.; Lyu, H.; Macreadie, L. K.; Ji, Z.; Zhang, Y.; Wang, B.; Haase, F.; Wöll, C.; Zaremba, O.; Andreo, J.; Wuttke, S.; Diercks, C. S. 25 Years of Reticular Chemistry. *Angew. Chem., Int. Ed.* **2021**, *60*, 23946−23974.

(9) Jhulki, S.; Evans, A. M.; Hao, X.-L.; Cooper, M. W.; Feriante, C. H.; Leisen, J.; Li, H.; Lam, D.; Hersam, M. C.; Barlow, S.; Brédas, J.-L.; Dichtel, W. R.; Marder, S. R. Humidity Sensing through Reversible Isomerization of a Covalent Organic Framework. *J. Am. Chem. Soc.* **2020**, *142*, 783−791.

(10) Feng, D.; Feng, Y.; Liu, Y.; Zhang, W.; Yan, Y.; Zhang, X. Thermal Conductivity of a 2D Covalent Organic Framework and Its Enhancement Using Fullerene 3D Self-Assembly: A Molecular Dynamics Simulation. *J. Phys. Chem. C* **2020**, *124*, 8386−8393.

(11) Moscarello, E. M.; Wooten, B. L.; Sajid, H.; Tichenor, L. D.; Heremans, J. P.; Addicoat, M. A.; McGrier, P. L. Thermal Conductivity of Two-Dimensional Benzobisoxazole-Linked Covalent Organic Frameworks with Nanopores: Implications for Thermal Management Applications. *ACS Appl. Nano Mater.* **2022**, *5*, 13787−13793.

(12) Freitas, S. K. S.; Borges, R. S.; Merlini, C.; Barra, G. M. O.; Esteves, P. M. Thermal Conductivity of Covalent Organic Frameworks as a Function of Their Pore Size. *J. Phys. Chem. C* **2017**, *121*, 27247−27252.

(13) Giri, A.; Hopkins, P. E. Heat Transfer Mechanisms and Tunable Thermal Conductivity Anisotropy in Two-Dimensional Covalent Organic Frameworks with Adsorbed Gases. *Nano Lett.* **2021**, *21*, 6188−6193.

(14) Guo, J.; Jiang, D. Covalent Organic Frameworks for Heterogeneous Catalysis: Principle, Current Status, and Challenges. *ACS Cent. Sci.* **2020**, *6*, 869−879.

(15) Chen, R.; Shi, J.-L.; Ma, Y.; Lin, G.; Lang, X.; Wang, C. Designed Synthesis of a 2D Porphyrin-Based Sp2 Carbon-Conjugated Covalent Organic Framework for Heterogeneous Photocatalysis. *Angew. Chem., Int. Ed.* **2019**, *58*, 6430−6434.

(16) Diercks, C. S.; Lin, S.; Kornienko, N.; Kapustin, E. A.; Nichols, E. M.; Zhu, C.; Zhao, Y.; Chang, C. J.; Yaghi, O. M. Reticular Electronic Tuning of Porphyrin Active Sites in Covalent Organic Frameworks for Electrocatalytic Carbon Dioxide Reduction. *J. Am. Chem. Soc.* **2018**, *140*, 1116−1122.

(17) Han, X.; Xia, Q.; Huang, J.; Liu, Y.; Tan, C.; Cui, Y. Chiral Covalent Organic Frameworks with High Chemical Stability for Heterogeneous Asymmetric Catalysis. *J. Am. Chem. Soc.* **2017**, *139*, 8693−8697.

(18) Wang, X.; Han, X.; Zhang, J.; Wu, X.; Liu, Y.; Cui, Y. Homochiral 2D Porous Covalent Organic Frameworks for Heterogeneous Asymmetric Catalysis. *J. Am. Chem. Soc.* **2016**, *138*, 12332−12335.

(19) Ascherl, L.; Evans, E. W.; Gorman, J.; Orsborne, S.; Bessinger, D.; Bein, T.; Friend, R. H.; Auras, F. Perylene-Based Covalent Organic Frameworks for Acid Vapor Sensing. *J. Am. Chem. Soc.* **2019**, *141*, 15693−15699.

(20) Gao, Q.; Li, X.; Ning, G.-H.; Leng, K.; Tian, B.; Liu, C.; Tang, W.; Xu, H.-S.; Loh, K. P. Highly Photoluminescent Two-Dimensional Imine-Based Covalent Organic Frameworks for Chemical Sensing. *Chem. Commun.* **2018**, *54*, 2349−2352.

(21) Li, Z.; Zhang, Y.; Xia, H.; Mu, Y.; Liu, X. A Robust and Luminescent Covalent Organic Framework as a Highly Sensitive and Selective Sensor for the Detection of Cu2+ Ions. *Chem. Commun.* **2016**, *52*, 6613−6616.

(22) Evans, A. M.; Strauss, M. J.; Corcos, A. R.; Hirani, Z.; Ji, W.; Hamachi, L. S.; Aguilar-Enriquez, X.; Chavez, A. D.; Smith, B. J.; Dichtel, W. R. Two-Dimensional Polymers and Polymerizations. *Chem. Rev.* **2022**, *122*, 442−564.

(23) Geng, K.; He, T.; Liu, R.; Dalapati, S.; Tan, K. T.; Tan, K. T.; Li, Z.; Li, Z.; Tao, S.; Tao, S.; Gong, Y.; Gong, Y.; Jiang, Q.; Jiang, D. Covalent Organic Frameworks: Design, Synthesis, and Functions. *Chem. Rev.* **2020**, *120*, 8814−8933.

(24) Alahakoon, S. B.; Diwakara, S. D.; Thompson, C. M.; Smaldone, R. A. Supramolecular Design in 2D Covalent Organic Frameworks. *Chem. Soc. Rev.* **2020**, *49*, 1344−1356.

(25) Huang, N.; Wang, P.; Jiang, D. Covalent Organic Frameworks: A Materials Platform for Structural and Functional Designs. *Nat. Rev. Mater.* **2016**, *1*, No. 16068.

(26) Smith, B. J.; Parent, L. R.; Overholts, A. C.; Beaucage, P. A.; Bisbey, R. P.; Chavez, A. D.; Hwang, N.; Park, C.; Evans, A. M.; Gianneschi, N. C.; Dichtel, W. R. Colloidal Covalent Organic Frameworks. *ACS Cent. Sci.* **2017**, *3*, 58−65.

(27) Kim, S.; Park, C.; Lee, M.; Song, I.; Kim, J.; Lee, M.; Jung, J.; Kim, Y.; Lim, H.; Choi, H. C. Rapid Photochemical Synthesis of Sea-Urchin-Shaped Hierarchical Porous COF-5 and Its Lithography-Free Patterned Growth. *Adv. Funct. Mat.* **2017**, *27*, No. 1700925.

(28) Kandambeth, S.; Venkatesh, V.; Shinde, D. B.; Kumari, S.; Halder, A.; Verma, S.; Banerjee, R. Self-Templated Chemically Stable Hollow Spherical Covalent Organic Framework. *Nat. Commun.* **2015**, *6*, No. 6786.

(29) Yin, Z.-J.; Xu, S.-Q.; Zhan, T.-G.; Qi, Q.-Y.; Wu, Z.-Q.; Zhao, X. Ultrahigh Volatile Iodine Uptake by Hollow Microspheres Formed from a Heteropore Covalent Organic Framework. *Chem. Commun.* **2017**, *53*, 7266−7269.

(30) Peng, Y.; Zhao, M.; Chen, B.; Zhang, Z.; Huang, Y.; Dai, F.; Lai, Z.; Cui, X.; Tan, C.; Zhang, H. Hybridization of MOFs and COFs: A New Strategy for Construction of MOF@COF Core-Shell Hybrid Materials. *Adv. Mater.* **2018**, *30*, No. 1705454.

(31) Zhang, G.; Tsujimoto, M.; Packwood, D.; Duong, N. T.; Nishiyama, Y.; Kadota, K.; Kitagawa, S.; Horike, S. Construction of a Hierarchical Architecture of Covalent Organic Frameworks via a Postsynthetic Approach. *J. Am. Chem. Soc.* **2018**, *140*, 2602−2609.

(32) Gole, B.; Stepanenko, V.; Rager, S.; Gruene, M.; Medina, D. D.; Bein, T.; Wuerthner, F.; Beuerle, F. Microtubular Self-Assembly of Covalent Organic Frameworks. *Angew. Chem., Int. Ed.* **2018**, *57*, 846−850.

(33) Natraj, A.; Ji, W.; Xin, J.; Castano, I.; Burke, D. W.; Evans, A. M.; Strauss, M. J.; Ateia, M.; Hamachi, L. S.; Gianneschi, N. C.; ALOthman, Z. A.; Sun, J.; Yusuf, K.; Dichtel, W. R. Single-Crystalline Imine-Linked Two-Dimensional Covalent Organic Frameworks Separate Benzene and Cyclohexane Efficiently. *J. Am. Chem. Soc.* **2022**, *144*, 19813−19824.

(34) Cisternas, L. A.; Vásquez, C. M.; Swaney, R. E. On the Design of Crystallization-Based Separation Processes: Review and Extension. *AIChE J.* **2006**, *52*, 1754−1769.

https://doi.org/10.1021/acs.chemmater.2c03448
Chem. Mater. XXXX, XXX, XXX−XXX

(35) Sun, S.; Lü, L.; Yang, A.; Wei, S.; Shen, W. Extractive Distillation: Advances in Conceptual Design, Solvent Selection, and Separation Strategies. *Chin. J. Chem. Eng.* **2019**, *27*, 1247−1256.
(36) Peng, Y.; Yang, W. 2D Metal-Organic Framework Materials for Membrane-Based Separation. *Adv. Mater. Interfaces* **2020**, *7*, No. 1901514.
(37) Tao, Z.-R.; Wu, J.-X.; Zhao, Y.-J.; Xu, M.; Tang, W.-Q.; Zhang, Q.-H.; Gu, L.; Liu, D.-H.; Gu, Z.-Y. Untwisted Restacking of Two-Dimensional Metal-Organic Framework Nanosheets for Highly Selective Isomer Separations. *Nat. Commun.* **2019**, *10*, No. 2911.
(38) Yusuf, K.; Shekhah, O.; ALOthman, Z.; Eddaoudi, M. Metal-Organic Frameworks Characterization via Inverse Pulse Gas Chromatography. *Appl. Sci.* **2021**, *11*, No. 10243.
(39) Yusuf, K.; Aqel, A.; ALOthman, Z. Metal-Organic Frameworks in Chromatography. *J. Chromatogr. A* **2014**, *1348*, 1−16.
(40) Broeckhoven, K.; Desmet, G. Advances and Innovations in Liquid Chromatography Stationary Phase Supports. *Anal. Chem.* **2021**, *93*, 257−272.
(41) Zhao, X.; Wang, Y.; Li, D.-S.; Bu, X.; Feng, P. Metal−Organic Frameworks for Separation. *Adv. Mater.* **2018**, *30*, No. 1705189.
(42) Cui, W.-G.; Hu, T.-L.; Bu, X.-H. Metal−Organic Framework Materials for the Separation and Purification of Light Hydrocarbons. *Adv. Mater.* **2020**, *32*, No. 1806445.
(43) Qian, H.-L.; Yang, C.-X.; Wang, W.-L.; Yang, C.; Yan, X.-P. Advances in Covalent Organic Frameworks in Separation Science. *J. Chromatogr. A* **2018**, *1542*, 1−18.
(44) Das, S.; Feng, J.; Wang, W. Covalent Organic Frameworks in Separation. *Annu. Rev. Chem. Biomol. Eng.* **2020**, *11*, 131−153.
(45) Wang, Z.; Zhang, S.; Chen, Y.; Zhang, Z.; Ma, S. Covalent Organic Frameworks for Separation Applications. *Chem. Soc. Rev.* **2020**, *49*, 708−735.
(46) Feng, J.; Feng, J.; Ji, X.; Li, C.; Han, S.; Sun, H.; Sun, M. Recent Advances of Covalent Organic Frameworks for Solid-Phase Microextraction. *TrAC, Trends Anal. Chem.* **2021**, *137*, No. 116208.
(47) Meng, S.-S.; Xu, M.; Han, T.; Gu, Y.-H.; Gu, Z.-Y. Regulating Metal−Organic Frameworks as Stationary Phases and Absorbents for Analytical Separations. *Anal. Methods* **2021**, *13*, 1318−1331.
(48) Tang, B.; Wang, W.; Hou, H.; Liu, Y.; Liu, Z.; Geng, L.; Sun, L.; Luo, A. A β-Cyclodextrin Covalent Organic Framework Used as a Chiral Stationary Phase for Chiral Separation in Gas Chromatography. *Chin. Chem. Lett.* **2022**, *33*, 898−902.
(49) Yang, C.-X.; Liu, C.; Cao, Y.-M.; Yan, X.-P. Facile Room-Temperature Solution-Phase Synthesis of a Spherical Covalent Organic Framework for High-Resolution Chromatographic Separation. *Chem. Commun.* **2015**, *51*, 12254−12257.
(50) Ji, Z.; Majors, R. E.; Guthrie, E. J. Porous Layer Open-Tubular Capillary Columns: Preparations, Applications and Future Directions. *J. Chromatogr. A* **1999**, *842*, 115−142.
(51) Ji, W.; Hamachi, L. S.; Natraj, A.; Flanders, N. C.; Li, R. L.; Chen, L. X.; Dichtel, W. R. Solvothermal Depolymerization and Recrystallization of Imine-Linked Two-Dimensional Covalent Organic Frameworks. *Chem. Sci.* **2021**, *12*, 16014−16022.
(52) Kazayawoko, M.; Balatinecz, J. J.; Romansky, M. Thermodynamics of Adsorption Ofn-Alkanes on Maleated Wood Fibers by Inverse Gas Chromatography. *J. Colloid Interface Sci.* **1997**, *190*, 408−415.
(53) Rankin, D. W. H. CRC handbook of chemistry and physics, 89th edition, edited by David R. Lide. *Crystallogr. Rev.* **2009**, *15*, 223−224.
(54) Luebbers, M. T.; Wu, T.; Shen, L.; Masel, R. I. Trends in the Adsorption of Volatile Organic Compounds in a Large-Pore Metal−Organic Framework, IRMOF-1. *Langmuir* **2010**, *26*, 11319−11329.
(55) Gutiérrez, I.; Díaz, E.; Vega, A.; Ordóñez, S. Consequences of Cavity Size and Chemical Environment on the Adsorption Properties of Isoreticular Metal-Organic Frameworks: An Inverse Gas Chromatography Study. *J. Chromatogr. A* **2013**, *1274*, 173−180.
(56) Grajek, H. Comparison of the Differential Isosteric Adsorption Enthalpies and Entropies Calculated from Chromatographic Data. *J. Chromatogr. A* **2003**, *986*, 89−99.
(57) Denayer, J. F.; Baron, G. V.; Martens, J. A.; Jacobs, P. A. Chromatographic Study of Adsorption of N-Alkanes on Zeolites at High Temperatures. *J. Phys. Chem. B* **1998**, *102*, 3077−3081.
(58) Korolev, A. A.; Shiryaeva, V. E.; Popova, T. P.; Kurganov, A. A. Enthalpy−Entropy Compensation Effect on Adsorption of Light Hydrocarbons on Monolithic Stationary Phases. *J. Sep. Sci.* **2011**, *34*, 2362−2369.
(59) Fowkes, F. M. Attractive Forces at Interfaces. *Ind. Eng. Chem.* **1964**, *56*, 40−52.
(60) Dorris, G. M.; Gray, D. G. Adsorption of N-Alkanes at Zero Surface Coverage on Cellulose Paper and Wood Fibers. *J. Colloid Interface Sci.* **1980**, *77*, 353−362.
(61) Schultz, J.; Lavielle, L.; Martin, C. The Role of the Interface in Carbon Fibre-Epoxy Composites. *J. Adhes.* **1987**, *23*, 45−60.
(62) Rieger, M.; Wittek, M.; Scherer, P.; Löbbecke, S.; Müller-Buschbaum, K. Preconcentration of Nitroalkanes with Archetype Metal−Organic Frameworks (MOFs) as Concept for a Sensitive Sensing of Explosives in the Gas Phase. *Adv. Funct. Mater.* **2018**, *28*, No. 1704250.
(63) Díaz, E.; Ordóñez, S.; Vega, A.; Coca, J. Adsorption Characterisation of Different Volatile Organic Compounds over Alumina, Zeolites and Activated Carbon Using Inverse Gas Chromatography. *J. Chromatogr. A* **2004**, *1049*, 139−146.
(64) Shi, B.; Wang, Y.; Jia, L. Comparison of Dorris−Gray and Schultz Methods for the Calculation of Surface Dispersive Free Energy by Inverse Gas Chromatography. *J. Chromatogr. A* **2011**, *1218*, 860−862.
(65) Rohrschneider, L. Chromatographic Characterization of Liquid Phases and Solutes for Column Selection and Identification. *J. Chromatogr. Sci.* **1973**, *11*, 160−166.
(66) Berthod, A.; Zhou, E. Y.; Le, K.; Armstrong, D. W. Determination and Use of Rohrschneider-McReynolds Constants for Chiral Stationary Phases Used in Capillary Gas Chromatography. *Anal. Chem.* **1995**, *67*, 849−857.
(67) Qian, H.-L.; Yang, C.-X.; Yan, X.-P. Bottom-up Synthesis of Chiral Covalent Organic Frameworks and Their Bound Capillaries for Chiral Separation. *Nat. Commun.* **2016**, *7*, No. 12104.
(68) Gu, Z.-Y.; Jiang, D.-Q.; Wang, H.-F.; Cui, X.-Y.; Yan, X.-P. Adsorption and Separation of Xylene Isomers and Ethylbenzene on Two Zn−Terephthalate Metal−Organic Frameworks. *J. Phys. Chem. C* **2010**, *114*, 311−316.
(69) Fan, L.; Yan, X.-P. Evaluation of Isostructural Metal−Organic Frameworks Coated Capillary Columns for the Gas Chromatographic Separation of Alkane Isomers. *Talanta* **2012**, *99*, 944−950.
(70) Wu, Y.-Y.; Yang, C.-X.; Yan, X.-P. An in Situ Growth Approach to the Fabrication of Zeolite Imidazolate Framework-90 Bonded Capillary Column for Gas Chromatography Separation. *Analyst* **2015**, *140*, 3107−3112.
(71) Lu, C.; Liu, S.; Xu, J.; Ding, Y.; Ouyang, G. Exploitation of a Microporous Organic Polymer as a Stationary Phase for Capillary Gas Chromatography. *Anal. Chim. Acta* **2016**, *902*, 205−211.
(72) Karwa, M.; Mitra, S. Gas Chromatography on Self-Assembled, Single-Walled Carbon Nanotubes. *Anal. Chem.* **2006**, *78*, 2064−2070.
(73) Yang, Y.-C.; Yoon, P.-R. Determination of Acid-Base Properties of Silicas by Inverse Gas Chromatography: Variation with Surface Treatment. *Mater. Trans.* **2007**, *48*, 1955−1960.
(74) Papirer, E.; Balard, H. Inverse Gas Chromatography: A Method for the Evaluation of the Interaction Potential of Solid Surfaces. *Interfacial Phenomena In Chromatography*, 1st ed.; CRC Press, 1999, pp 154−172.
(75) Donnet, J. B.; Park, S. J.; Balard, H. Evaluation of Specific Interactions of Solid Surfaces by Inverse Gas Chromatography. *Chromatographia* **1991**, *31*, 434−440.

https://doi.org/10.1021/acs.chemmater.2c03448
Chem. Mater. XXXX, XXX, XXX−XXX